

Article

# Improving Corrosion Resistance and Biocompatibility of Magnesium Alloy by Sodium Hydroxide and Hydrofluoric Acid Treatments

Chang-Jiang Pan <sup>1,\*†</sup>, Li-Qun Pang <sup>2,†</sup>, Yu Hou <sup>1</sup>, Yue-Bin Lin <sup>1</sup>, Tao Gong <sup>1</sup>, Tao Liu <sup>1</sup>, Wei Ye <sup>1</sup> and Hong-Yan Ding <sup>1</sup>

<sup>1</sup> Jiangsu Provincial Key Lab for Interventional Medical Devices, Huaiyin Institute of Technology, Huai'an 223003, China; houyu0807@sina.com (Y.H.); lybztyt@hyit.edu.cn (Y.-B.L.); gtao208@163.com (T.G.); liutao0214@hyit.edu.cn (T.L.); weiye\_ciac@126.com (W.Y.); dhy@hyit.edu.cn (H.-Y.D.)

<sup>2</sup> Department of General Surgery, Huai'an First People's Hospital, Nanjing Medical University, Huai'an 223300, China; panglq@163.com

\* Correspondence: panchangjiang@hyit.edu.cn; Tel.: +86-517-8355-9150

† These authors contributed equally to this work and should be considered co-first authors.

Academic Editor: Hidenori Otsuka

Received: 21 November 2016; Accepted: 22 December 2016; Published: 28 December 2016

**Abstract:** Owing to excellent mechanical property and biodegradation, magnesium-based alloys have been widely investigated for temporary implants such as cardiovascular stent and bone graft; however, the fast biodegradation in physiological environment and the limited surface biocompatibility hinder their clinical applications. In the present study, magnesium alloy was treated by sodium hydroxide (NaOH) and hydrogen fluoride (HF) solutions, respectively, to produce the chemical conversion layers with the aim of improving the corrosion resistance and biocompatibility. The results of attenuated total reflectance Fourier transform infrared spectroscopy (ATR-FTIR) and X-ray photoelectron spectroscopy (XPS) indicated that the chemical conversion layers of magnesium hydroxide or magnesium fluoride were obtained successfully. Sodium hydroxide treatment can significantly enhance the surface hydrophilicity while hydrogen fluoride treatment improved the surface hydrophobicity. Both the chemical conversion layers can obviously improve the corrosion resistance of the pristine magnesium alloy. Due to the hydrophobicity of magnesium fluoride, HF-treated magnesium alloy showed the relative better corrosion resistance than that of NaOH-treated substrate. According to the results of hemolysis assay and platelet adhesion, the chemical surface modified samples exhibited improved blood compatibility as compared to the pristine magnesium alloy. Furthermore, the chemical surface modified samples improved cytocompatibility to endothelial cells, the cells had better cell adhesion and proliferative profiles on the modified surfaces. Due to the excellent hydrophilicity, the NaOH-treated substrate displayed better blood compatibility and cytocompatibility to endothelial cells than that of HF-treated sample. It was considered that the method of the present study can be used for the surface modification of the magnesium alloy to enhance the corrosion resistance and biocompatibility.

**Keywords:** magnesium alloy; chemical surface modification; blood compatibility; cytocompatibility; endothelial cell

## 1. Introduction

Magnesium and its alloys are attracting more and more attention as kinds of biodegradable metallic biomaterials due to their excellent mechanical properties and biodegradation [1–3], specifically in the applications that require degradation and subsequent disappearance of the device after cure [4]. For example, magnesium-based alloys are very suitable for bone graft because the Young's modulus

and density are very close to human natural bone. On the other side, Mg and its alloys are good candidates for cardiovascular stents due to their good biocompatibility and biodegradation [5]. Furthermore, the addition of some elements such as Zn into magnesium alloys can also impart excellent antibacterial properties and thus make them suitable for antibacterial biomaterials [6]. Nevertheless, it is still a big challenge to control the corrosion rates while at the same time maintain good biocompatibility. The adverse effects caused by the fast *in vivo* adsorption after the implantation, such as excessive hydrogen production [7], local alkalization [8], enrichment of magnesium ions and the second corrosion products, etc., can result in the premature loss of the mechanical strength and thus prevent or delay the tissue healing, finally leading to implanting failure. On the other side, in most cases, the magnesium alloy surface has a lack of bioactivities because there are no any biomolecules or chemical groups on its surface; consequently, the surface biocompatibility need to be improved before clinical usage. Immobilization of biomolecules on biomaterials' surfaces represents one of the most popular and effective ways to improve the surface biocompatibility. However, direct surface biofunctionalization of the magnesium alloy may not be possible because of the fast degradation in the physiological environment; therefore, in most cases, the control of corrosion rate should be considered firstly so that the implant can maintain the sufficient mechanical properties before tissue healing.

It is well known that both the corrosion and tissue-biomaterials interfacial biological reactions are surface phenomena. In most instances, surface properties play a determined role in the corrosion resistance and the biocompatibility of the magnesium alloys. Accordingly, surface modification has been one of the most important and effective methods to improve the corrosion resistance and the biocompatibility [9]. To date, numerous surface modification techniques have been developed to improve the biocompatibility and the corrosion resistance of the magnesium-based alloys, including surface alloying [10], surface chemical treatment [11], fabrication of surface coating [12], plasma treatment [13], self-assembly [14], micro-arc oxidation [15], anodization [16], plasma electrolytic oxidation [17], etc. In addition, a recent study reported that a hybrid materials of poly (ether imide) (PEI)-silica nanoparticles can be coated on the Mg surface to improve the corrosion stability and implant-tissue interfaces of magnesium substrates [18], and the results indicated that the content of silica can modulate the corrosion rate and biocompatibility and the authors stated that the hybrid systems have significant potential as a coating material of Mg for load-bearing orthopedic applications. Among these methods, formation of a chemical conversion layer via chemical surface modification is a simple and cost-effective method and has been increasingly used to improve the corrosion resistance and biocompatibility of magnesium alloy. Generally speaking, chemical surface modification includes alkaline treatment [19], fluoride treatment [20], phosphating [21], anodization [22], ion implantation [23], etc., all of which are associated with the replacement of the natively forming, and not particularly the corrosion resistant oxide layer on the surface of the Mg substrate [24]. By chemical surface modification, a dense and stable chemical conversion layer can be produced on the magnesium alloys. The layer can isolate the substrate from the corrosion medium, and thus improve the corrosion resistance and significantly reduce the adverse effects caused by the fast degradation. In the past several decades, many studies have been performed to investigate the corrosion behaviors and corrosion mechanism in the different corrosion mediums; however, relatively less literature reported the biocompatibility of the chemical surface modified magnesium alloy, especially when it is used for cardiovascular implants.

The aim of the present study is to investigate the corrosion behaviors and biocompatibility of the chemical surface modified magnesium alloy. To this end, two chemical surface modification methods, i.e., sodium hydroxide (NaOH) treatment and hydrofluoric acid (HF) treatment, were used to modify the magnesium alloy surface to enhance the corrosion resistance. The blood compatibility and interactions with endothelial cells were further investigated.

## 2. Materials and Methods

### 2.1. Formation of the Chemical Conversion Layers

The AZ31B magnesium alloy rod (compositions: 3.19% Al, 0.81% Zn, 0.334% Mn, 0.02% Si, 0.005% Fe, 0.05% Cu, 0.04% Ca, 0.1% Be, Mg rest, Dongguan You'an Metal Materials Co., Ltd., Dongguan, China) was cut into 2 mm thick plates and then polished to the mirror surface using abrasive paper from 600# to 2000#. After ultrasonically cleaned 10 min in acetone (Sinopharm Chemical Reagent Co., Ltd, Huai'an, China), ethanol (Sinopharm Chemical Reagent Co., Ltd, Huai'an, China), respectively, the sample was immersed into a 3 M NaOH solution (Sinopharm Chemical Reagent Co., Ltd, Huai'an, China) for 24 h in a 75 °C water bath. The sample was cleaned with plenty of distilled water and dried by the compressed air flow. The obtained sample was labeled as Mg–OH.

For HF treatment, the sample was firstly treated 15 min by the mixture solution of NaOH (50 g/L) and Na<sub>3</sub>PO<sub>4</sub>·12H<sub>2</sub>O (10 g/L, Sinopharm Chemical Reagent Co., Ltd, Huai'an, China) at room temperature. Subsequently, the sample was cleaned and immersed into an HF solution (12 mol/L) for another 15 min. The sample was cleaned by the distilled water and dried by the compressed air flow. The HF treated sample was labeled as Mg–HF.

### 2.2. Surface Characterization

The surface chemical structures after the chemical surface modification was firstly investigated by a TENSOR 27 (Bruker, Karlsruhe, Germany) ATR-FTIR with a grazing angle reflector and the high-sensitivity detector. The experiment was carried out under atmospheric pressure and at room temperature. The infrared spectra between 4000–650 cm<sup>-1</sup> was plotted.

In order to further examine the surface chemical structures of the pristine magnesium alloy and the chemical conversion layers, X-ray photoelectron spectroscopy (XPS, VG Scientific, East Grinstead, UK) was utilized to detect the surface atomic concentrations of the different samples. The focused monochromatic Mg K<sub>α</sub> X-ray source was used for excitation. The experiment was carried at 14 kV and the measurement pressure was 8 × 10<sup>-8</sup> Pa. The take-off angle was kept at 30° and the atomic information between 0 and 1200 eV was recorded. The surface atomic concentrations were calculated through the software provided by the XPS supplier (Avantage XPS).

The water contact angle was used to characterize the surface hydrophilicity and the experiments were carried out on a DSA25 contact angle goniometer (Krüss GmbH, Nürnberg, Germany) at room temperature. A sessile drop method was applied to measure the water contact angle. After cleaning and drying the samples, 10 μL of distilled water was dropped on the substrate and the liquid drop image was immediately taken. The water contact angle was obtained by the software provided by Krüss GmbH (Drop Shape Analysis, DSA Version 1.92, Krüss GmbH, Nürnberg, Germany). Five parallel samples were measured and the values were averaged and expressed as mean ± standard deviation (SD).

### 2.3. Corrosion Behaviors

#### 2.3.1. Potentiodynamic Polarization Curve

The potentiodynamic polarization curves were plotted to characterize the electrochemical behaviors of different samples in simulated body fluid (SBF, compositions: NaCl, 8 g/L; KCl, 0.4 g/L; NaHCO<sub>3</sub>, 0.35 g/L; CaCl<sub>2</sub>, 0.14 g/L; Na<sub>2</sub>HPO<sub>4</sub>, 0.06 g/L; KH<sub>2</sub>PO<sub>4</sub>, 0.06 g/L; MgSO<sub>4</sub>·7H<sub>2</sub>O, 0.01 g/L; glucose, 1 g/L; Sinopharm Chemical Reagent Co., Ltd, Huai'an, China). The pH value of the corrosion medium was adjusted to 7.4 using an NaOH solution. The SBF solution was kept at 37 ± 0.5 °C during the experiment. The experiments were carried out on a CHI660D electrochemical workstation (CHI Instruments, Inc., Shanghai, China). A three-electrode system (CHI Instruments, Inc., Shanghai, China) was used to measure the polarization curve. The sample, saturated Ag/AgCl electrode and the platinum electrode were the working electrode, reference electrode and the auxiliary electrode,

respectively. Before the experiment, the samples were encapsulated by epoxy resin using Cu wire, as the conducting wire and the exposed area for each sample was about 1.13 cm<sup>2</sup>. The sample was immersed into the SBF solution until the open circuit potential became stable. The polarization curves were measured with the scanning rate of 10 mV/s. The corrosion current and corrosion potential were determined according to the polarization curve.

### 2.3.2. Immersion Test

The immersion test was applied to further evaluate the in vitro corrosion behaviors of the pristine magnesium alloy and the modified magnesium alloys in SBF solution. The sample was firstly encapsulated using silicon rubber to expose the 1 cm<sup>2</sup> area and subsequently immersed into 25 mL SBF solution (pH 7.4) at 37 °C for 1, 5, 7 days, respectively. After the pre-determined period, the sample was taken out and washed with distilled water. The sample was dried and then a thin gold layer was sputter-coated for the surface morphology observation by scanning electron microscopy (SEM, FEI Quata 250, Hillsboro, OR, USA).

## 2.4. Anticoagulation

### 2.4.1. Hemolysis Rate

The hemolysis experiments were done in accordance with ISO 10993-4:2009 and ASTM F756-00. The fresh whole blood was obtained legally from a healthy volunteer and mixed with 3.8 wt % sodium citrate solution with the ratio of 9:1. The blood was centrifuged at 1500 rev/min to obtain the red blood cells, and then 2 mL red blood cells was diluted to get 2% erythrocyte suspension using physiological saline solution. The sample was incubated 1 h at 37 °C with 10 mL erythrocyte suspension. After taking out the sample, the medium was centrifuged at 3000 rev for 10 min. The absorbance of the supernatant was measured at 540 nm by a microplate reader (Eons, Bio-Tek, Winooski, VT, USA). For controls, the mixture of 2 mL erythrocyte and 98 mL physiological saline was used as the negative control, and the mixture of 2 mL erythrocyte and 98 mL ultrapure water was used as the positive control. The hemolysis ratio was calculated according to the following formula:

$$R = (A - C1)/(C2 - C1) \times 100\%,$$

where  $R$  is the hemolysis ratio (%),  $A$  is the absorbance of the sample,  $C1$  is the absorbance of the negative control (%), and  $C2$  is the absorbance of the positive control.

### 2.4.2. Platelet Adhesion

Platelet-Rich plasma (PRP) was prepared by centrifuging the fresh whole blood containing 3.8 wt % sodium citrate at 1500 rev/min for 15 min. The sample was incubated with 0.5 mL of PRP at 37 °C for 2 h and then rinsed three times with phosphate buffer saline (PBS) to remove any weakly adherent platelets. The adherent platelets were fixed in a 2% glutaraldehyde solution for 12 h. Subsequently, the samples were dehydrated using the graded ethanol and dried in atmosphere. After being sputter-coated with a thin gold layer, the adhered platelets were observed by a scanning electron microscope (SEM, FEI Quata 250).

## 2.5. Endothelial Cell Behaviors

### 2.5.1. Cell Adhesion

The samples were firstly sterilized by ultraviolet light and then placed into the 24-well cell culture plate. In addition, 1.5 mL of  $5 \times 10^4$  cells/mL endothelial cell (HUVEC, ECV304, Cobioer, Nanjing, China) suspension was seeded on the substrate and incubated 6 and 24 h at 37 °C, respectively, in a humidified atmosphere containing 5% CO<sub>2</sub>. The cell culture medium was DMEM/F-12 (Hyclone)

supplemented with 10% fetal bovine serum and 1% penicillin streptomycin. After that, the sample was washed two times by PBS, the attached cells were fixed 2 h by 2.5% glutaraldehyde solution (Sinopharm Chemical Reagent Co., Ltd, Huai'an, China). In order to observe the cell adhesion by fluorescent microscopy, the cells were stained successively by rhodamine and 4',6-diamidino-2-phenylindole (DAPI, Sigma, Shanghai, China). To this end, 100  $\mu$ L rhodamine solution (10  $\mu$ g/mL, Sigma, Shanghai, China) was added on the sample surface and incubated for 30 min. After being washed twice by the physiological saline, 100  $\mu$ L of DAPI solution was dropped on the sample surface for incubating for 15 min. The sample was washed twice again by the physiological saline and dried in the atmospheric pressure. The adhered cells were observed by an inverted fluorescent microscopy (Carl Zeiss A2, Jena, Germany).

### 2.5.2. CCK-8

The proliferative profiles of endothelial cells on the different samples were characterized by a CCK-8 assay. In brief, the samples were firstly cleaned and sterilized for 5 h by ultraviolet light. Subsequently, 1 mL of  $5 \times 10^4$  cells/mL endothelial cells (HUVEC, ECV304) was seeded on the sample surface and incubated 24 h at 37 °C. The cell culture medium was DMEM/F-12 (Hyclone) supplemented with 10% fetal bovine serum and 1% penicillin streptomycin. After removing the culture medium, the sample was rinsed three times by the sterilized PBS. Furthermore, 20  $\mu$ L CCK-8 solution and 200  $\mu$ L DMEM culture medium were added on the sample and incubated 4 h at 37 °C. The absorbance of the medium was measured by a microplate reader (Biotek Eons, Winooski, VT, USA) at 450 nm. Triplicate parallel samples were measured and the values were averaged for each sample.

### 2.6. Statistical Analysis

For the results of CCK-8, hemolysis rate and water contact angle, the statistical significance between the sample groups was assessed using one-way Analysis of Variance (ANOVA). A value of  $p < 0.05$  was considered statistically significant.

## 3. Results and Discussion

### 3.1. Attenuated Total Reflectance Fourier Transform Infrared Spectroscopy (ATR-FTIR) and X-ray Photoelectron Spectroscopy (XPS)

The surface chemical structures after the chemical surface modification were firstly characterized by ATR-FTIR. As shown in Figure 1, no infrared adsorption was observed on the pristine magnesium alloy surface, indicating that there were no chemical groups on the pristine magnesium alloy surface. After sodium hydroxide treatment, a sharp peak at 3700  $\text{cm}^{-1}$  can be found, which can be attributed to the adsorption of hydroxyls, suggesting that a significant amount of hydroxyls was introduced on the surface after NaOH treatment [25] and a chemical layer of  $\text{Mg}(\text{OH})_2$  was produced on the substrate. The hydroxyls make the following surface functionalization possible. In our recent study, we demonstrated that the self-assembly can be carried out on the NaOH-treated Mg surface, which can be used to immobilize the biomolecules for improving biocompatibility [26]. For the hydrogen fluoride treated sample, it can be clearly seen that no hydroxyls can be detected and there were two new peaks at 900 and 720  $\text{cm}^{-1}$ , demonstrating that a magnesium fluoride layer was produced after HF treatment.

XPS was utilized to further detect the surface atomic concentration of the different samples. Figure 2 shows the XPS survey spectra of the different samples. The element concentrations were listed in Table 1. It can be clearly seen that the peaks of  $\text{C}_{1s}$  and  $\text{O}_{1s}$  can be found on the curve of the pristine magnesium alloy expect  $\text{Mg}_{1s}$  and  $\text{Al}_{2p}$ , indicating that there was carbon contamination on the surface and the magnesium alloy was oxidized naturally. After sodium hydroxide treatment, the oxygen concentration increased significantly while the concentration of  $\text{Mg}_{1s}$  decreased obviously (Table 1), suggesting that more oxygen has been introduced on the magnesium surface. These oxygen

elements can react with magnesium to form the magnesium hydroxide layer, which can isolate the substrate from the corrosion medium and thus enhance the corrosion resistance. After hydrogen fluoride treatment, a strong  $F_{1s}$  peak was observed on the curve of Mg-HF. At the same time, the oxygen concentration decreased significantly, indicating that the newly formed magnesium fluoride layer replaced the natively forming oxide layer on the surface of the Mg substrate.

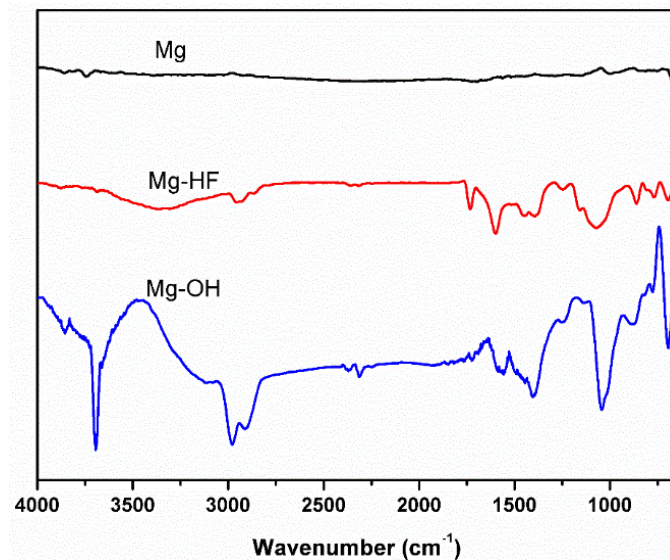


**Figure 1.** Attenuated total reflectance Fourier transform infrared spectroscopy (ATR-FTIR) spectra of the pristine magnesium alloy and chemical treated samples.

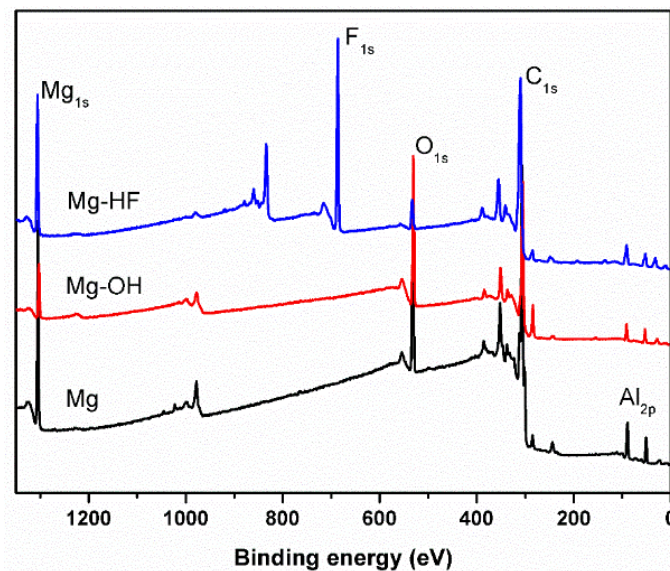


**Figure 2.** The survey X-ray photoelectron spectroscopy (XPS) spectra for different samples.

**Table 1.** X-ray photoelectron spectroscopy (XPS) surface atom percentage of different samples (wt %).

Samples	Mg	C	O	F	Al	Zn
Mg	42.05	12.72	43.22	-	1.47	0.54
Mg-OH	22.15	22.87	54.12	-	0.86	-
Mg-HF	28.19	25.96	8.94	35.97	0.94	-

### 3.2. Surface Hydrophilicity

The surface hydrophilicity was characterized by the water contact angle. As shown in Figure 3, it can be seen that the pristine magnesium alloy exhibited relative hydrophobicity and its water contact angle was about  $86.8^\circ$ . After sodium hydroxide treatment, the water contact angle was reduced to about  $21.6^\circ$ , indicating that the hydrophilicity was enhanced obviously. According to the FTIR results, more hydrophilic hydroxyls can be introduced on the surface after NaOH treatment, which can significantly enhance the surface hydrophilicity. In contrast, as compared to the pristine magnesium alloy, the water contact angle was increased to  $103.7^\circ$  after HF treatment, suggesting that hydrogen fluoride treatment can enhance the surface hydrophobicity. It was considered that the magnesium fluoride layer contributed to the improved hydrophobicity. Therefore, the excellent hydrophilic chemical conversion layer can be produced by sodium hydroxide treatment, while a relative hydrophobic chemical conversion layer can be obtained after hydrogen fluoride treatment. In the following studies, the influences of different hydrophilicity on corrosion behaviors, blood compatibility and endothelial cell behaviors were explored in the present study.

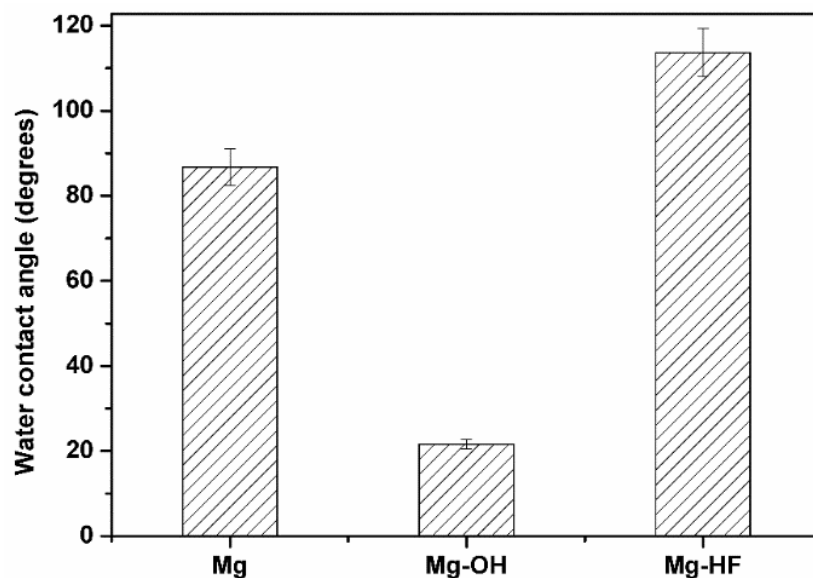


**Figure 3.** The water contact angles of different samples. Five parallel samples were measured and the values were averaged. The data were expressed as mean  $\pm$  standard deviation (SD). The value of Mg-OH was significantly lower ( $p < 0.05$ ) than that of the pristine magnesium alloy, while the water contact angle of Mg-HF was significantly larger ( $p < 0.05$ ) than that of the pristine magnesium alloy.

### 3.3. Corrosion Behaviors

The corrosion behaviors were firstly investigated by the potentiodynamic polarization and the results are shown in Figure 4. The corresponding corrosion parameters are shown in Table 2. Generally speaking, corrosion potential ( $E_{\text{corr}}$ ) reflects the corrosion tendency while corrosion current density ( $i_{\text{corr}}$ ) represents the corrosion rate. Under the same conditions, the sample with larger corrosion potential is generally more difficult to corrode than the sample with lower corrosion potential. As shown in Figure 4 and Table 2, when compared to the chemical treatment substrates, the pristine magnesium alloy showed the lowest corrosion potential ( $-1.57$  V) and the largest corrosion current density ( $37.26 \mu\text{A}/\text{cm}^2$ ), suggesting that the unmodified magnesium alloy can easily corrode in SBF, and its corrosion rate was the largest. After chemical surface modification, the corrosion potential shifted to  $-1.174$  V (Mg-OH) and  $-1.128$  V (Mg-HF), respectively, indicating that both chemical surface modification methods can reduce the corrosion tendency of magnesium alloy. It was considered that the chemical conversion layers were dense and stable and their microstructure were favorable

for the improvement of the corrosion resistance. On the other side, as shown in Table 2, the corrosion current densities were reduced to  $2.05 \mu\text{A}/\text{cm}^2$  (Mg–OH) and  $0.68 \mu\text{A}/\text{cm}^2$  (Mg–HF) after surface modification and these values were significantly lower than that of the pristine magnesium alloy ( $37.26 \mu\text{A}/\text{cm}^2$ ), demonstrating that the chemical surface modification can significantly enhance the corrosion resistance of magnesium alloy. According to the previous FTIR and XPS results, the newly formed chemical conversion layers ( $\text{Mg}(\text{OH})_2$  or  $\text{MgF}_2$ ) replaced the loosely native oxide layer on the magnesium alloy substrate, which provide the barriers to isolate the corrosion medium from the magnesium substrate, and therefore leading to better corrosion resistance.

**Table 2.** The corrosion potentials and corrosion current densities of different samples.

Samples	$E_{\text{corr}}$ (V)	$i_{\text{corr}}$ ( $\text{A}\cdot\text{cm}^{-2}$ )
AZ31B	−1.570	$3.726 \times 10^{-5}$
Mg–OH	−1.174	$2.052 \times 10^{-6}$
Mg–HF	−1.128	$6.821 \times 10^{-7}$

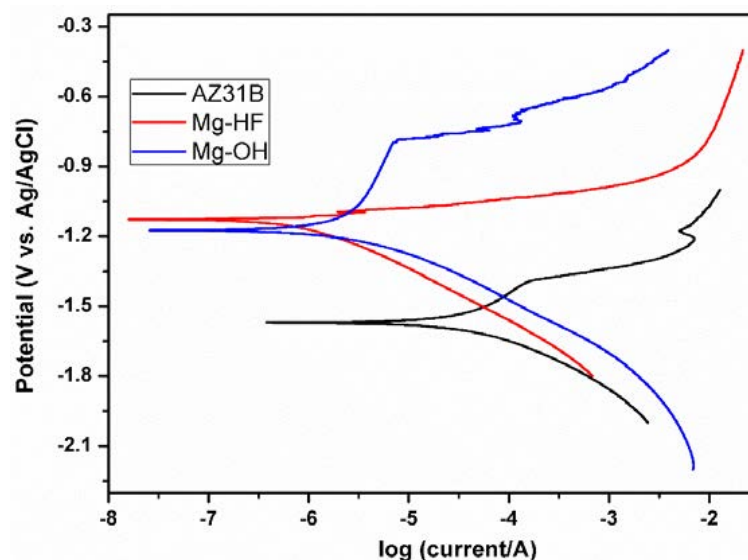


**Figure 4.** Potentiodynamic polarization curves of different samples in simulated body fluid (SBF) solution at  $37^\circ\text{C}$ .

In addition, it can be seen from Figure 4 and Table 2 that Mg–HF showed better corrosion resistance than Mg–OH because the former had relative larger corrosion potential and smaller corrosion current density. As shown in Figure 5, the surface of the substrate treated by HF showed the relatively smooth morphology while the morphology of Mg–OH was relatively rough. The rough surface can increase the contact area with corrosion medium, consequently leading to smaller corrosion resistance than that of Mg–HF. In addition, the dense microstructure of magnesium fluoride may also contribute to the enhanced corrosion resistance. On the other side, it is well known that the fluoride element generally exhibits hydrophobicity. The magnesium fluoride layer can not only resist the substrate from the corrosion medium but also provide a hydrophobic surface to prevent the corrosion ions from penetrating into the magnesium substrate, leading to the enhanced corrosion resistance.

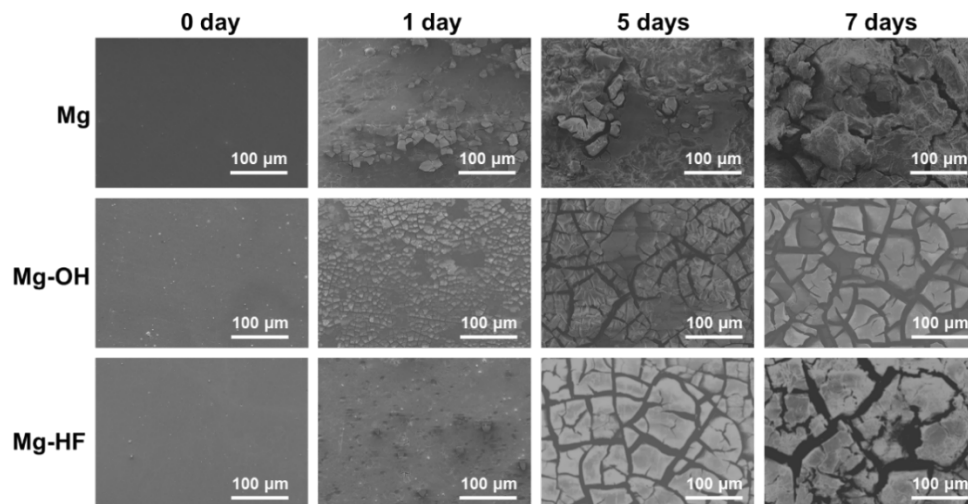


**Figure 5.** The typical scanning electron microscope (SEM) images of the different samples immersed into SBF solution for one day, five days and seven days, respectively.

The corrosion behaviors were further investigated by the immersion test. The samples were immersed into SBF solution for different times and then the surface morphologies were observed by SEM. The typical SEM images of the different samples immersed in SBF solution for one, five, and seven days, respectively, are shown in Figure 5. The pristine magnesium displayed a relatively smooth surface while the other two modified samples exhibited relatively rough surface morphologies due to the surface chemical treatment. As compared to Mg–OH, the surface of Mg–HF displayed smoother morphology, which contributed to the improved corrosion resistance because the rough surface can increase the contact area with corrosion medium. On the other side, the relatively smooth surface of Mg–HF also suggested that the chemical conversion layer of magnesium fluoride was denser than that of Mg–OH, which could contribute to better corrosion resistance. More corrosion products can be clearly found on the pristine magnesium alloy surface only after immersing the sample in SBF for one day when compared to the modified samples, indicating that the unmodified magnesium alloy had a poor anticorrosion. After being immersed in SBF for five and seven days, a larger amount of corrosion products can be observed, indicating that a serious corrosion occurred on the pristine Mg substrate. In contrast, no obvious corrosion products were found on the chemical treated surfaces, demonstrating that the corrosion resistance can be effectively improved by the chemical surface modification. It was considered that the chemical conversion layer can prevent the corrosion ions from penetrating the surface of the magnesium substrate. However, the obvious cracks can be observed on the chemical treated surfaces. After one-day immersion, almost no corrosion cracks were found on the Mg–HF surface while the relatively small cracks can be found on the Mg–OH surface, indicating that Mg–HF showed better corrosion resistance than Mg–OH. After being immersed into SBF for five and seven days, respectively, it can be clearly seen that the corrosion cracks became larger on both chemical treatment surfaces, indicating the occurrence of corrosion. However, the corrosion was not serious as compared to the pristine magnesium alloy.

### 3.4. Anticoagulation

Red blood cells (erythrocyte) are the major components of human blood. When the human blood comes into contact with implants, the erythrocytes may be destroyed and activated, finally resulting in the occurrence of hemolysis and clotting [27]. Therefore, it is generally expected that the blood-contacting biomaterials have a low hemolysis rate. According to the Chinese standard, a material is acceptable and can be used for blood-contacting biomaterials when the hemolysis rate is below 5%. The hemolysis rates of the different samples are shown in Figure 6. As compared to the

modified samples, the pristine magnesium alloy exhibited the largest hemolysis rate and the value was as high as 59%, indicating that a serious hemolysis occurred. It was considered that the high hemolysis rate is closely related to the local alkalization induced by the fast corrosion of the pristine magnesium alloy. A recent piece of literature reported that the high pH value caused by the fast degradation of magnesium alloy can lead to a high hemolysis ratio [28]. On the other side, a high pH value can increase the binding ability of hemoglobin to the membrane and subsequently increase the hemolysis rate, and the red blood cells can fuse with  $\text{Ca}^{2+}$  of the medium, thus resulting in a rupture of erythrocytes, finally leading to serious hemolysis [29]. According to our previous study, the pH value was as high as 8.5 when the pristine magnesium alloy was immersed into SBF for two days [26], and the higher pH value can be obtained when the sample was immersed into SBF for more time. In addition, rapid release of magnesium ions from its fast corrosion is also related to severe hemolysis reaction [30]. Consequently, serious hemolysis can occur on the pristine magnesium alloy due to its fast degradation. After the chemical surface modification, it can be clearly seen that the hemolysis rate decreased significantly; however, there was no significant difference between Mg–HF and Mg–OH. As discussed above, both chemical surface modification methods can obviously enhance the corrosion resistance and reduce the corrosion rate. Our previous study indicated that the pH value of Mg–OH was significantly smaller than that of the pristine magnesium alloy [24] when they were immersed into a corrosion medium for the same time, which contributed to the lower hemolysis rates of the modified samples. However, it was noticeable that the hemolysis rate was larger than 5%, indicating that the modified samples may not be suitable for the blood-contacting biomaterials, although the chemical surface modification can significantly reduce the hemolysis rate. Therefore, it is necessary to further modify the surface properties with other approaches, such as the immobilization of biomolecules, to reduce the hemolysis rate.

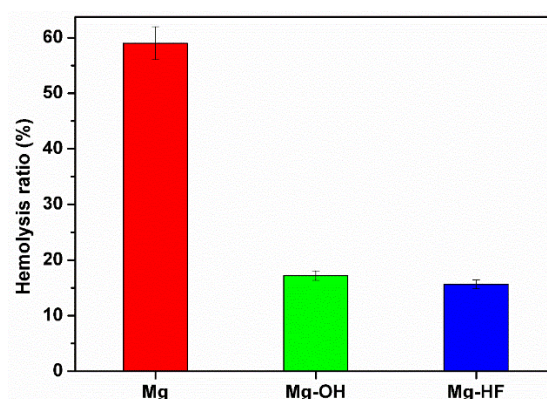


**Figure 6.** The hemolysis rate for different samples. Three parallel samples were measured and the data were averaged and expressed as mean  $\pm$  SD. The hemolysis rates of the modified samples were significantly lower ( $p < 0.05$ ) than that of the unmodified magnesium alloy. There was no significant difference ( $p > 0.05$ ) between Mg–OH and Mg–HF.

Generally speaking, human plasma proteins firstly adsorb in seconds to the biomaterials surface when a biomaterial makes contact with blood [31]. Subsequently, the platelets will be attached on the surface followed by complement activation and other blood cell responses, finally leading to thrombus formation [32]. Consequently, the platelets have been considered as a major cause of thrombosis, and platelet adhesion represents the popular approach to characterize the blood compatibility of biomaterials [33]. The typical SEM images of the platelets adhered to the different samples were shown in Figure 7. Obviously, more platelets can be observed on the pristine magnesium alloy surface (Figure 7a). At the same time, some aggregated platelets were also observed and these aggregated platelets may be further activated, indicating that the pristine magnesium alloy had relative poor anticoagulation. The platelets on the pristine magnesium alloy surface extended their pseudopods

(Figure 7d). In contrast, the number of platelets adhered to the Mg–OH and Mg–HF was obviously reduced (Figure 7b,c), no aggregated and activated platelets were observed, and the morphologies of the attached platelets display a more intact and typical disk-like shape (Figure 7e,f), indicating that both chemical surface modification can improve the anticoagulation of the magnesium alloys. In general, the excellent hydrophilic surface has low surface free energy, and it can prevent plasma protein and platelet adhesion, therefore improving the blood compatibility. The magnesium alloy treated by sodium hydroxide treatment had excellent hydrophilicity; therefore, the number of adhered platelets decreased significantly as compared to the pristine magnesium, and no aggregated platelets were found. For Mg–HF, a relative hydrophobic surface was achieved, which can reduce the ability of the surface to adsorb platelet and therefore enhance the anticoagulation.

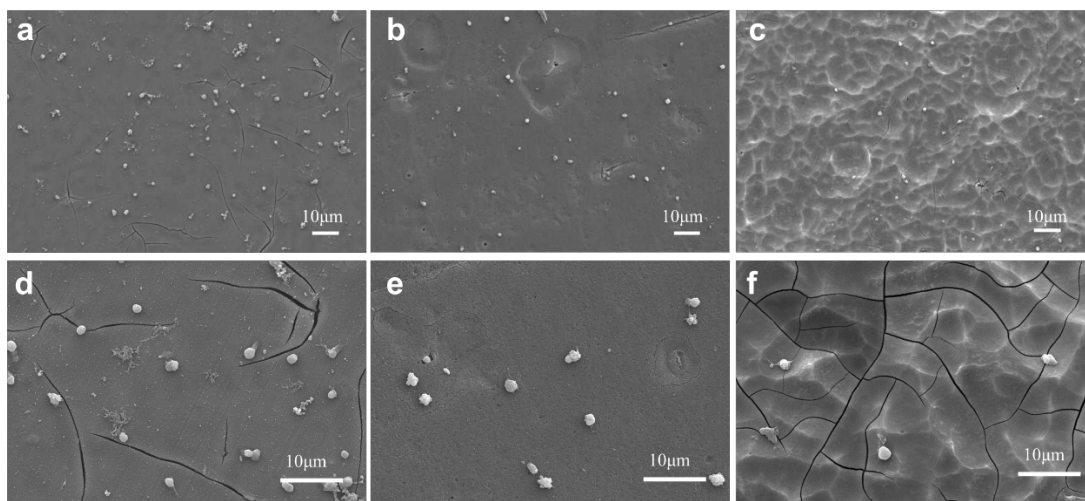


**Figure 7.** The typical SEM images of the adhered platelets on AZ31B (a,d), Mg–OH (b,e) and Mg–HF (c,f).

### 3.5. Interactions with Endothelial Cells

Vascular endothelium is a thin layer of simple endothelial cells, which forms an interface between circulating blood in the lumen and the rest of the vessel wall. Endothelial dysfunction, or the loss of proper endothelial function, is often regarded as a key early event in the development of atherosclerosis [34]. For the blood contacting materials or devices such as intravascular stents, the inserted devices or materials inevitably cause the damage of endothelium and thus lead to endothelial cell dysfunction. Therefore, endothelial cell behaviors on these implants surfaces play an important role in the *in vivo* performances. Magnesium alloy has been intensively investigated as a cardiovascular stent; therefore, endothelial cell adhesion was investigated in the present study. Figure 8 shows the typical fluorescent images of the endothelial cells adhered to the different substrates. Because the cell adhesion mainly occurs with 24 h, the amount of the adhered cells had no obvious change after six and 24 h cultures for the same sample. Nevertheless, the cells exhibited better spread shapes on the substrates after 24 h culture, suggesting that the adhered cells can sense the surroundings to extend their pseudopod to spread on the surface. As compared to the pristine magnesium, more cells can be observed on the chemical modified surfaces, demonstrating that the surface chemical modification can enhance the cell adhesion. Because cells are very sensitive to environmental fluctuations, any dramatic physical and chemical changes around them can produce deleterious and sometimes fatal effects [35,36]. As shown by our results, the corrosion of magnesium could cause pH increase and release of a significant amount of magnesium ions, resulting in the environment changes of cells and thus leading to poor cell adhesion on the pristine Mg substrate. On the other side, proper reduction of the degradation rate of magnesium alloy not only creates a relatively stable interface for cell adhesion

and growth but also retards the release of corrosion products to reduce the cytotoxicity, therefore finally resulting in the enhanced cytocompatibility [37]. It was reported that passivation of the Mg surface in 1 M NaOH, which forms the  $Mg(OH)_2$  passivation layer, can strongly enhance cell survival and adhesion [38]. Our results indicated that both of the NaOH and HF treatments can improve the corrosion of Mg alloys and thus promote cell adhesion. Although the number of adhered cells on Mg–OH had no difference with Mg–HF; however, it can be seen that the attached cells on Mg–OH displayed typical cobblestone morphology, while the cells on Mg–HF and the pristine magnesium alloy had relative shrinkage shape, indicating that cells on Mg–OH had better spreading.

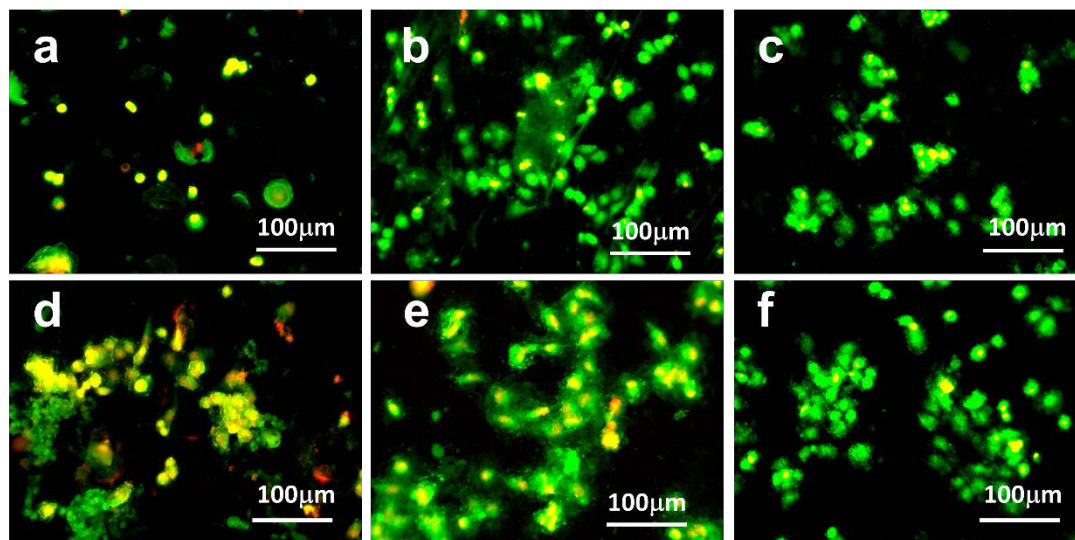


**Figure 8.** The typical fluorescent images of endothelial cells adhered on AZ31B (a,d), Mg–OH (b,e) and Mg–HF (c,f). The cells were cultured with samples for 6 h (a–c), 24 h (d–f), respectively. (yellow, nuclei; green, cytoskeleton).

It is well known that the proliferation percentage of cells on a surface indicates the cytocompatibility of a substrate, which is useful in determining the potential biomedical applications of the substrate [39]. In the present study, endothelial cell proliferation was investigated by the CCK-8 method, and the results are summarized in Figure 9. Clearly, more cells could be found on Mg–OH and Mg–HF as compared to the pristine magnesium alloy, indicating that the chemical conversion layer can promote cell proliferation to some degree. According to the corrosion mechanism of magnesium alloy, the fast degradation can produce a larger amount of  $OH^-$  and thus cause high local alkalization, which may severely affect the pH-dependent physiological processes such as cell adhesion and proliferation. After chemical surface modification, a chemical conversion layer with the improved corrosion resistance can be produced, which can reduce the corrosion rate and thus reduce the pH change, leading to better cell proliferation. For example, fluoride treatment of magnesium or its alloys leads to the replacement of original oxide film with a thin and more homogeneous layer of  $MgF_2$  with higher polarization resistance. The advantages of newly formed layers are their high density, lower water solubility, and the harmlessness of the release of fluorine ions into the organism. On the other side, it was found from Figure 9 that the absorbance of Mg–OH was larger than that of Mg–HF, suggesting that the growth and proliferation of endothelial cells on Mg–OH were better than that of on Mg–HF. Although the modified surface cannot produce extracellular matrix (ECM) protein for cell attachment and proliferation, the cells can grow well on the hydrophilic surface, as compared to the cells on the hydrophobic Mg–HF surface. In general, cell growth on the hydrophilic surfaces is usually more efficient than on the hydrophobic surface. In this case, cell adhesion can also occur through non-receptor chemical binding, such as electrostatic, ionic-polar interactions, and hydrogen binding to surface functional groups [40]. As shown in the results of ATR-FTIR and XPS,

a larger amount of hydroxyl can be introduced on the surface and an excellent hydrophilic surface can be achieved. Cell attachment can occur through hydrogen binding between hydroxyl and cells, leading to better cell adhesion. The adhered cells can synthesize and deposit their own extracellular matrix proteins on Mg–OH for further cell proliferation. The hydrophobic Mg–HF surface cannot interact with cells by the non-receptor binding because it was lacking any reactive groups; however, the hydrophobic surface may adsorb the protein from culture medium and thus promote cell adhesion and proliferation. Consequently, the cell proliferation on Mg–HF was a little bit poorer than Mg–OH.

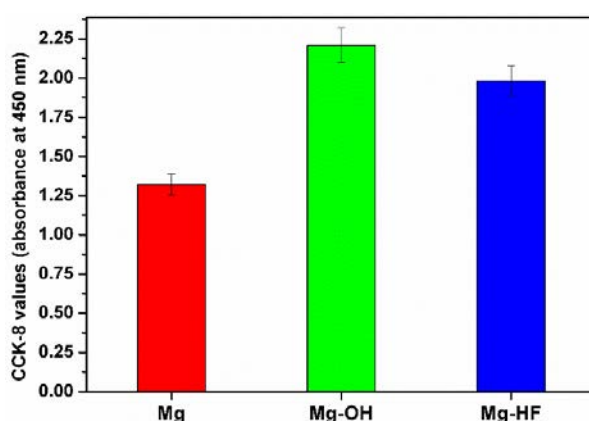


**Figure 9.** Endothelial cell proliferation characterized by CCK-8 assay for different samples. Data for each sample were taken from three parallel samples, and are expressed as mean  $\pm$  SD. The absorbance values of the modified samples are significantly larger ( $p < 0.05$ ) than that of the pristine magnesium alloy.

#### 4. Conclusions

The magnesium alloy was successfully modified by sodium hydroxide and hydrogen fluoride, and the chemical conversion layers of magnesium hydroxide and magnesium fluoride were successfully obtained. Sodium hydroxide can significantly enhance surface hydrophilicity while HF treatment improved the surface hydrophobicity. Both chemical surface modification approaches can significantly improve the corrosion resistance of the magnesium alloy. Owing to its hydrophobicity and relatively smooth surface, Mg–HF had relatively better corrosion resistance than Mg–OH. Due to the surface chemical structure changes and the improved corrosion resistance, the anticoagulation and endothelial cell adhesion and proliferation were enhanced after the chemical surface modification. However, the sample modified by sodium hydroxide showed the better anticoagulation and cytocompatibility to endothelial cells than the HF-modified substrate. The method of the present study can be used for the surface modification of the magnesium alloy to enhance the corrosion resistance and biocompatibility.

**Acknowledgments:** The authors acknowledge the financial support from the Natural Science Foundation of China (31470926, 31500778), the Jiangsu Qing Lan Project, the Six Talent Peaks Project of Jiangsu Province, and the Natural Science Foundation of Huaiyin Institute of Technology (15HGZ003).

**Author Contributions:** Chang-Jiang Pan and Li-Qun Pang conceived and designed the experiments; Yu Hou performed the surface chemical treatment experiments; Yue-Bin Lin performed FTIR and XPS experiments and analyzed the data. Tao Liu and Wei Ye performed the anticoagulation characterization. Tao Gong performed the cell experiments. Chang-Jiang Pan and Hong-Yan Ding wrote the paper.

**Conflicts of Interest:** The authors declare no conflict of interest.

#### References

- Walker, J.; Shadanbaz, S.; Woodfield, T.B.F.; Staiger, M.P.; Dias, G.J. Magnesium biomaterials for orthopedic application: A review from biological perspective. *J. Biomed. Mater. Res. Part B Appl. Biomater.* **2014**, *102B*, 1316–1331. [[CrossRef](#)] [[PubMed](#)]

2. Manivasagam, G.; Suwas, S. Biodegradable Mg and Mg based alloys for biomedical implants. *Mater. Sci. Technol.* **2014**, *30*, 515–520. [[CrossRef](#)]
3. Gu, X.N.; Li, S.S.; Li, X.M.; Fan, Y.B. Magnesium based degradable biomaterials: A review. *Front. Mater. Sci.* **2014**, *8*, 200–218. [[CrossRef](#)]
4. Stainger, M.P.; Pietak, A.M.; Huadmai, J.; Dias, G. Magnesium and its alloys as orthopedic biomaterials: A review. *Biomaterials* **2006**, *27*, 1728–1734. [[CrossRef](#)] [[PubMed](#)]
5. Zhang, E.; Shen, F. Blood compatibility of a ferulic acid (FA)-eluting PHBHHx system for biodegradable magnesium stent application. *Mater. Sci. Eng. C Mater. Biol. Appl.* **2015**, *52*, 37–45. [[CrossRef](#)] [[PubMed](#)]
6. He, G.; Wu, Y.; Zhang, Y.; Zhu, Y.; Liu, Y.; Li, M.; Zheng, G.; He, B.; Yin, Q.; Zheng, Y.; et al. Addition of Zn to the ternary Mg-Ca-Sr alloys significantly improves their antibacterial properties. *J. Mater. Chem. B* **2015**, *3*, 6676–6689. [[CrossRef](#)] [[PubMed](#)]
7. Williams, D. New interests in magnesium. *Med. Device Technol.* **2006**, *17*, 9–10. [[PubMed](#)]
8. Song, G. Control of biodegradation of biocompatible magnesium alloys. *Corros. Sci.* **2007**, *49*, 1696–1701. [[CrossRef](#)]
9. Yang, J.; Cui, F.; Lee, I.S. Surface modifications of magnesium alloys for biomedical applications. *Ann. Biomed. Eng.* **2011**, *39*, 1857–1871. [[CrossRef](#)] [[PubMed](#)]
10. Savalani, M.M.; Pizarro, J.M. Effect of preheat and layer thickness on selective laser melting (SLM) of magnesium. *Rapid Prototyp. J.* **2016**, *22*, 115–122. [[CrossRef](#)]
11. Hu, L.; Meng, Q.; Chen, S.; Wang, H. Effect of Zn content on the chemical conversion treatments of AZ91D magnesium alloy. *Appl. Surf. Sci.* **2012**, *259*, 816–823. [[CrossRef](#)]
12. Kannan, M.B.; Walter, R.; Yamamoto, A. Biocompatibility and in vitro degradation behavior of magnesium-calcium alloy coated with calcium phosphate using an unconventional electrolyte. *ACS Biomater. Sci. Eng.* **2016**, *2*, 56–64. [[CrossRef](#)]
13. Yang, J.; Cui, F.Z.; Lee, I.S.; Wang, X. Plasma surface modification of magnesium alloy for biomedical application. *Surf. Coat. Technol.* **2010**, *205*, 5182–5187. [[CrossRef](#)]
14. Ye, S.H.; Jang, Y.S.; Yun, Y.H.; Shankarraman, V.; Woolley, J.R.; Hong, Y.; Gamble, L.J.; Ishihara, K.; Wagner, W.R. Surface modification of a biodegradable magnesium alloy with phosphorylcholine (PC) and sulfobetaine (SB) functional macromolecules for reduced thrombogenicity and acute corrosion resistance. *Langmuir* **2013**, *29*, 8320–8327. [[CrossRef](#)] [[PubMed](#)]
15. Li, Y.; Lu, F.; Li, H.L.; Zhu, W.J.; Pan, H.B.; Tan, G.X.; Lao, Y.H.; Ning, C.Y.; Ni, G.X. Corrosion mechanism of micro-arc oxidation treated biocompatible AZ31 magnesium alloy in simulated body fluid. *Prog. Nat. Sci. Mater. Int.* **2014**, *24*, 516–522. [[CrossRef](#)]
16. Xue, D.; Yun, Y.; Schulz, M.J.; Shanov, V. Corrosion protection of biodegradable magnesium implants using anodization. *Mater. Sci. Eng. C Mater. Biol. Appl.* **2011**, *31*, 215–223. [[CrossRef](#)]
17. Gnedenkov, S.V.; Sharkeev, Y.P.; Sinebryukhov, S.L.; Khrisanova, O.A.; Legostaeva, E.V.; Zavidnaya, A.G.; Puz, A.V.; Khlusov, I.A.; Opra, D.P. Functional coatings formed on the titanium and magnesium alloys as implant materials by plasma electrolytic oxidation technology: Fundamental principles and synthesis conditions. *Corros. Rev.* **2016**, *34*, 65–83. [[CrossRef](#)]
18. Kang, M.H.; Jang, T.S.; Jung, H.D.; Kim, S.M.; Kim, H.E.; Koh, Y.H.; Song, J. Poly (ether imide)-silica hybrid coatings for tunable corrosion behavior and improved biocompatibility of magnesium implants. *Biomed. Mater.* **2016**, *11*, 035003. [[CrossRef](#)] [[PubMed](#)]
19. Jeong, H.; Yoo, Y. Synthesis and characterization of thin films on magnesium alloy using a hydrothermal method. *Surf. Coat. Technol.* **2015**, *284*, 26–30. [[CrossRef](#)]
20. Mao, L.; Shen, L.; Chen, J.H.; Wu, Y.; Kwak, M.; Lu, Y.; Xue, Q.; Pei, J.; Zhang, L.; Yuan, G.Y.; et al. Enhanced bioactivity of Mg-Nd-Zn-Zr alloy achieved with nanoscale MgF<sub>2</sub> surface for vascular stent application. *ACS Appl. Mater. Interfaces* **2015**, *7*, 5320–5330. [[CrossRef](#)] [[PubMed](#)]
21. Xu, L.P.; Zhang, E.L.; Yang, K. Phosphating treatment and corrosion properties of Mg-Mn-Zn alloy for biomedical application. *J. Mater. Sci. Mater. Med.* **2009**, *20*, 859–867. [[CrossRef](#)] [[PubMed](#)]
22. Mousa, H.M.; Hussein, K.H.; Woo, H.M.; Park, C.H.; Kim, C.S. One-Step anodization deposition of anticorrosive bioceramic compounds on AZ31B magnesium alloy for biomedical application. *Ceram. Int.* **2015**, *41*, 10861–10870. [[CrossRef](#)]
23. Xu, R.; Wu, G.; Yang, X.; Hu, T.; Lu, Q.; Chu, P.K. Controllable degradation of biomedical magnesium by chromium and oxygen dual ion implantation. *Mater. Lett.* **2011**, *65*, 2171–2173. [[CrossRef](#)]

24. Wang, J.; Tang, J.; Zhang, P.; Li, Y.; Lai, Y.; Qin, L. Surface modifications of magnesium alloys developed for bioabsorbable orthopedic implants: A general review. *J. Biomed. Mater. Res. B Appl. Biomater.* **2012**, *100B*, 1691–1701. [[CrossRef](#)] [[PubMed](#)]
25. Chen, Y.; Wan, G.; Wang, J.; Zhao, S.; Zhao, Y.; Huang, N. Covalent immobilization of phytic acid on Mg by alkaline pre-treatment: Corrosion and degradation behavior in phosphate buffered saline. *Corros. Sci.* **2013**, *75*, 280–286. [[CrossRef](#)]
26. Pan, C.J.; Hou, Y.; Wang, Y.N.; Gao, F.; Liu, T.; Hou, Y.H.; Zhu, Y.F.; Ye, W.; Wang, L.R. Effects of self-assembly of 3-phosphonopropionic acid, 3-aminopropyltrimethoxysilane and dopamine on the corrosion behaviors and biocompatibility of a magnesium alloy. *Mater. Sci. Eng. C Mater. Biol. Appl.* **2016**, *67*, 132–143. [[CrossRef](#)] [[PubMed](#)]
27. Pan, C.J.; Hou, Y.H.; Zhang, B.B.; Dong, Y.X.; Ding, H.Y. Blood compatibility and interaction with endothelial cells of titanium modified by sequential immobilization of poly (ethylene glycol) and heparin. *J. Mater. Chem. B* **2014**, *2*, 892–902. [[CrossRef](#)]
28. Zhen, Z.; Liu, X.; Huang, T.; Xi, T.; Zheng, Y. Hemolysis and cytotoxicity mechanisms of biodegradable magnesium and its alloys. *Mater. Sci. Eng. C Mater. Biol. Appl.* **2015**, *46*, 202–206. [[CrossRef](#)] [[PubMed](#)]
29. Kang, I.K.; Kwon, O.H.; Lee, Y.M.; Yong, K.S. Preparation and surface characterization of functional group-grafted and heparin-immobilized polyurethanes by plasma glow discharge. *Biomaterials* **1996**, *17*, 841–847. [[CrossRef](#)]
30. Gorbet, M.B.; Sefton, M.V. Biomaterial-associated thrombosis: Role of coagulation factors, complement, platelets and leukocytes. *Biomaterials* **2004**, *25*, 5681–5703. [[CrossRef](#)] [[PubMed](#)]
31. Koh, L.B.; Rodriguez, I.; Venkatraman, S.S. The effect of topography of polymer surfaces on platelet adhesion. *Biomaterials* **2010**, *31*, 1533–1545. [[CrossRef](#)] [[PubMed](#)]
32. Sask, K.N.; McClung, W.G.; Berry, L.R.; Chan, A.K.C.; Brash, J.L. Immobilization of an antithrombin-heparin complex on gold: Anticoagulation properties and platelet interactions. *Acta Biomater.* **2011**, *7*, 2029–2034. [[CrossRef](#)] [[PubMed](#)]
33. Wu, K.K. Platelet activation mechanisms and markers in arterial thrombosis. *J. Intern. Med.* **1996**, *239*, 17–34. [[CrossRef](#)] [[PubMed](#)]
34. Sitia, S.; Tomasoni, L.; Atzeni, F.; Ambrosio, G.; Cordiano, C.; Catapano, A.; Tramontana, S.; Perticone, F.; Naccarato, P.; Camici, P.; et al. From endothelial dysfunction to atherosclerosis. *Autoimmun. Rev.* **2010**, *9*, 830–834. [[CrossRef](#)] [[PubMed](#)]
35. Xin, Y.C.; Jiang, J.; Huo, K.F.; Tang, G.Y.; Chu, P.K. Corrosion resistance and cytocompatibility of biodegradable surgical magnesium alloy coated with hydrogenated amorphous silicon. *J. Biomed. Mater. Res. A* **2009**, *89A*, 717–726. [[CrossRef](#)] [[PubMed](#)]
36. Witte, F.; Hort, N.; Vogt, C.; Cohen, S.; Kainer, K.U.; Willumeit, R.; Feyerabend, F. Degradable biomaterials based on magnesium corrosion. *Curr. Opin. Solid State Mater. Sci.* **2008**, *12*, 63–72. [[CrossRef](#)]
37. Zhao, Y.; Wu, G.; Jiang, J.; Wong, H.M.; Yeung, K.W.K.; Chu, P.K. Improved corrosion resistance and cytocompatibility of magnesium alloy by two-stage cooling in thermal treatment. *Corros. Sci.* **2012**, *59*, 360–365. [[CrossRef](#)]
38. Lorenz, C.; Brunner, J.G.; Kollmannsberger, P.; Jaafar, L.; Fabry, B.; Virtanen, S. Effect of surface pre-treatments on biocompatibility of magnesium. *Acta Biomater.* **2009**, *5*, 2783–2789. [[CrossRef](#)] [[PubMed](#)]
39. Benhabbour, S.R.; Sheardown, H.; Adronov, A. Cell adhesion and proliferation on hydrophilic dendritically modified surfaces. *Biomaterials* **2008**, *29*, 4177–4186. [[CrossRef](#)] [[PubMed](#)]
40. Bacáková, L.; Mares, V.; Bottone, M.G.; Pellicciari, C.; Lisá, V.; Svorčík, V. Fluorine ion-implanted polystyrene improves growth and viability of vascular smooth muscle cells in culture. *J. Biomed. Mater. Res.* **2000**, *49*, 369–379. [[CrossRef](#)]

